Journal of Ultrafine Grained and Nanostructured Materials
https://jufgnsm.ut.ac.ir
Vol. 58, No.2, June 2025, pp. 152-160
Print ISSN: 2423-6845 Online ISSN: 2423-6837
DOI: 10.22059/jufgnsm.2025.02.03

Engineering Photocatalytic $TiO_2/CuWO_4$ Coatings: The Synergistic Effect of Oxidants on Heavy Metal Remediation

Hamed Bahramian*, Arash Fattah-alhosseini*, Minoo Karbasi

Bu-Ali Sina University, Department of Materials Engineering, Faculty of Engineering, Hamedan, Iran

Recieved: 11 November 2025; Accepted: 23 November 2025

**Corresponding authors, E-mail:* hamedbahramian1377@gmail.com , a.fattah@basu.ac.ir

ABSTRACT

A highly active $TiO_2/CuWO_4$ heterostructure coating for Cr^{6+} photoreduction was developed through PEO and hydrothermal post-treatment. Characterizations such as FESEM, GXRD, AFM and wettability, revealed that nano-sized $CuWO_4$ integration transforms the morphology, producing a hierarchical, microporous base with uniformly distributed particles and a super-hydrophilic, rough surface for improved accessibility. Oxidant screening revealed that both radical ($SO_4^{\bullet-}$, $HO^{\bullet}$) and non-radical species are critical to the mechanism. Peroxydisulfate (PDS) achieved the highest synergy (synergistic factor= 0.9) via sulfate radical generation, significantly outperforming peroxymonosulfate (PMS) and the ineffective H_2O_2. This study proposes a dual-pathway mechanism and introduces a durable, scalable photocatalytic coating solution for environmental cleanup.

Keywords: *Cr photoreduction, Oxidants, plasma electrolytic oxidation, hydrothermal, $TiO_2/CuWO_4$ Coatings.*

1. Introduction

Rapid urban and industrial expansion has significantly intensified water contamination through the persistent discharge of hazardous materials [1-3]. A particularly severe global environmental concern is the presence of hexavalent chromium Cr^{6+} in water supplies, which ranks among the most perilous pollutants. To address this, numerous conventional and advanced techniques for Cr^{6+} removal from wastewater have been established, each with its own set of benefits and drawbacks [4,5]. In the last ten years, semiconductor-based photocatalysis has emerged as a promising strategy for environmental cleanup, especially in treating wastewater. This approach is further enhanced by the inclusion of oxidants, which are crucial for degrading aqueous pollutants more effectively [6]. On the other hand, oxidizing agents such as peroxymonosulfate (PMS), peroxydisulfate (PDS), and hydrogen peroxide (H_2O_2) boost photocatalytic performance by facilitating the creation of reactive oxygen species (ROS) and improving the separation of photogenerated charges [7,8]. Titanium dioxide (TiO_2) is a widely studied photocatalyst, valued for its cost-effectiveness, chemical stability, potent oxidizing ability, non-toxic nature, and biocompatibility, establishing it as a standard material in environmental and energy

technologies [9]. Nonetheless, its widespread use is hindered by a large bandgap that restricts light absorption to ultraviolet wavelengths and a tendency for rapid recombination of electron-hole pairs, which diminishes quantum yield [10,11]. To overcome these shortcomings, strategies such as heterojunction engineering have been adopted to make TiO_2 responsive to visible light and to improve the separation of charge carriers [12-14]. Copper tungstate ($CuWO_4$), an n-type semiconductor, has gained interest due to its promising electronic and optical properties for photocatalysis. While photocatalysts in powder form provide high reactivity, their real-world utility is hampered by difficulties in retrieval, low reusability, and a tendency for particles to clump together, which blocks active sites and impedes light. Consequently, research has shifted towards immobilized photocatalytic coatings as a more viable solution. Depositing the photocatalyst as a thin film onto a support material offers multiple benefits: it increases stability and reusability, allows for optimized light absorption through controlled thickness, prevents particle aggregation, and simplifies the process of separating the catalyst from the purified water [15]. Plasma Electrolytic Oxidation (PEO) is noted as a particularly effective method for producing TiO_2-based photocatalytic coatings, as it can generate porous, strongly adhered, and customizable surfaces [16,17]. Recent improvements in PEO coatings involve both pre- and post-treatment methods. Pre-treatments condition the substrate to enhance coating quality, whereas post-treatments, such as hydrothermal processing, alter the coating's structure to create nanostructures that significantly increase photocatalytic activity [12,18,19].

To better understand the photocatalytic reduction mechanism of chromium, this study used various scavengers and oxidants, as detailed earlier, to analyze the behavior of the hydrothermally post-treated PEO-synthesized $TiO_2/CuWO_4$ photocatalyst.

2. Experimental

2.1. Chemicals and substrates

A Ti substrate with dimensions of 20×15×1 mm was used; its chemical composition has been reported elsewhere [20]. Potassium hydroxide (KOH), sodium phosphate dodecahydrate ($Na_3PO_4{\cdot}12H_2O$), sodium tungstate (Na_2WO_4) and copper(II) acetate ($Cu(CH_3COO)_2$) were purchased from Merck Co. (Germany). Additionally, potassium chromate (K_2CrO_4) as pollutant, scavengers, and oxidants such as methanol (CH_3OH), sodium pyruvate ($C_3H_3NaO_3$), (tert-butanol ($C_4H_{10}O$), peroxymonosulfate (KH_SO_5 PMS), hydrogen peroxide (H_2O_2), and peroxydisulfate ($K_2S_2O_8$, PDS) procured from Sigma-Aldrich (USA).

2.2. Production of the coatings

Prior to the PEO process, the titanium sheets were prepared by sequential grinding with abrasive papers, followed by ultrasonic cleaning in distilled water and acetone for five minutes each, and finally air-drying. The PEO was performed using a pulsed DC power supply. The Ti substrates, acting as the anode, were fully immersed in an electrolyte solution contained in a stainless-steel vessel that served as the cathode. A water-cooling system was used to maintain the electrolyte temperature below 40 °C during the process. The specific PEO parameters were selected based on our previous work [21], (electrical parameters: duty cycle=80, frequency=1000 Hz, time=10 min, current density= 12 A/dm^2, electrolyte= 5 gr/L Na_3PO_4 and 4 gr/L KOH) and the resulting sample is designated as "T."

The hydrothermal post-treatment, adapted from Hang et al. [22] with modifications, was employed to grow crystalline $CuWO_4$ nanoparticles on the TiO_2 coating. Briefly, 0.3 M Na_2WO_4 and 0.3 M $Cu(CH_3COO)_2$ were dissolved in 40 mL of deionized water under magnetic stirring for one hour, forming a sky-blue suspension. This solution was transferred to a Teflon-lined autoclave, where the T sample was placed on a holder. The sealed autoclave was then heated at 180 °C for 24 hours. The final product is labeled as "TC."

2.3. Characterization of the coatings

A suite of characterization techniques was employed to analyze the coatings. Field-emission scanning electron microscopy (FE-SEM) revealed the morphology and elemental distribution. Surface wettability was assessed via static water contact angle measurements, while X-ray diffraction (XRD) with CuKα radiation, including grazing incidence mode, determined the crystalline structure. Atomic force microscopy (AFM) mapped the surface topography and measured roughness. The photocatalytic activity (PA) of the coatings was evaluated by measuring the reduction of hexavalent chromium (Cr^{6+}) under visible light at room temperature. Prior to illumination, the coatings (with a surface area of 3 cm^2) were immersed in 30 mL of a 5 ppm Cr^{6+} solution and stirred in the dark for 30 minutes to establish adsorption-desorption equilibrium. Subsequently, the solution containing the samples was irradiated using a 100 W visible LED lamp. During the photocatalytic reaction, 0.5 mL aliquots were collected from the reactor at regular intervals from 1 to 6 hours. The concentration of Cr^{6+} was specifically determined by the diphenylcarbazide method [4]. For this test, a 0.5 mL sample was mixed with 2 mL of deionized water, 0.04 mL of H_2SO_4 (10% v/v), and a diphenylcarbazide solution (0.65% w/w in acetone). The absorbance of the resulting solution was measured at 540 nm using

a Teksan-lena SB-G100 spectrophotometer. The influence of oxidants was studied by adding 5 mM of H_2O_2, PMS ($KHSO_5$), or PDS ($K_2S_2O_8$). To probe the reaction mechanism, methanol and tert-butanol (TBA) at 0.01 M and sodium pyruvate (9.1 mM) acted as scavengers for hydroxyl, sulfate radicals and H_2O_2, respectively.

3. Result and discussion

As shown in Fig. 1, the TC and T coatings both possess the porous, sponge-like morphology inherent to the PEO fabrication process, which is caused by gas evolution and the rapid quenching of molten oxide [23]. The key morphological distinction is the successful incorporation of well-dispersed Copper tungstate ($CuWO_4$) nanoparticles within the porous network of the TC coating, achieved through hydrothermal modification.

Fig. 2 displays the grazing-angle XRD patterns, which confirm the successful hydrothermal modification. Both the T and TC coatings are primarily composed of anatase TiO_2 (ICDD 00-071-1167), with titanium substrate peaks (ICDD 00-088-2321) visible due to the thin, porous oxide layer [24]. The defining feature of the TC coating's pattern is the presence of new peaks that match the reference for triclinic $CuWO_4$ (ICDD 00-080-1918), conclusively identifying the product of the hydrothermal treatment as crystalline copper tungstate.

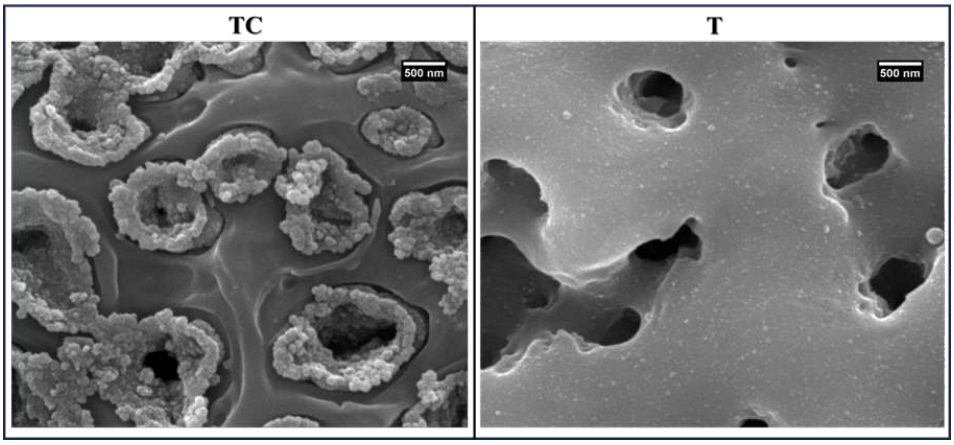

Fig. 1- FESEM micrographs of coatings [20].

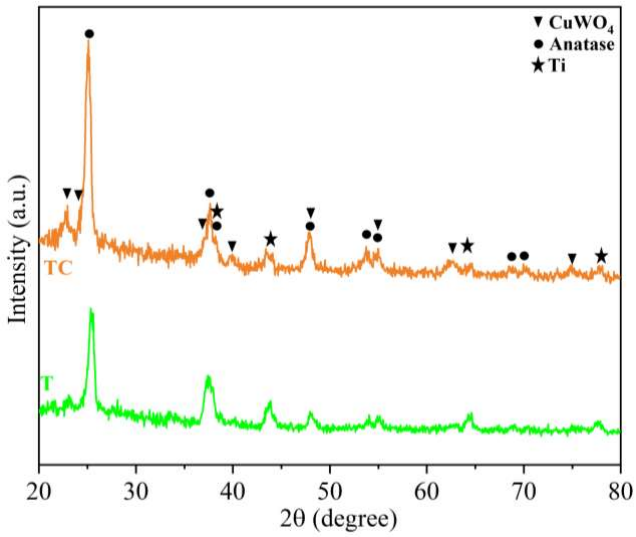

Fig. 2- GXRD patterns of T and TC coatings [20].

AFM topography analysis (Fig. 3) indicates that the hydrothermal process uniformly deposited $CuWO_4$ particles on the coating, resulting in a substantial increase in average roughness (R_a) from 31.75 nm to 75.94 nm.

As shown in Fig. 4, the hydrothermally modified TC coating displayed superhydrophilic behavior with an unmeasurable contact angle, a significant improvement over the 85° angle of the pristine T coating. This phenomenon is consistent with the established principle that surface roughness is a key determinant of wettability [25]. The increased roughness of the TC coating, quantified by AFM, enhances water spreading by reducing interfacial tension.

The photoreduction efficiency of Cr^{6+} using various oxidants, including peroxymonosulfate (PMS), peroxydisulfate (PDS), and hydrogen peroxide (H_2O_2) is presented in Fig. 5(a). As observed, the addition of PDS significantly enhanced the photoreduction process. This outcome aligns with mechanisms reported in prior studies [8], as a greater amount of PDS is converted into sulfate radicals $SO_4^{\bullet-}$ under acidic conditions, such as the experimental pH of 5.5. Below are the chemical reactions for

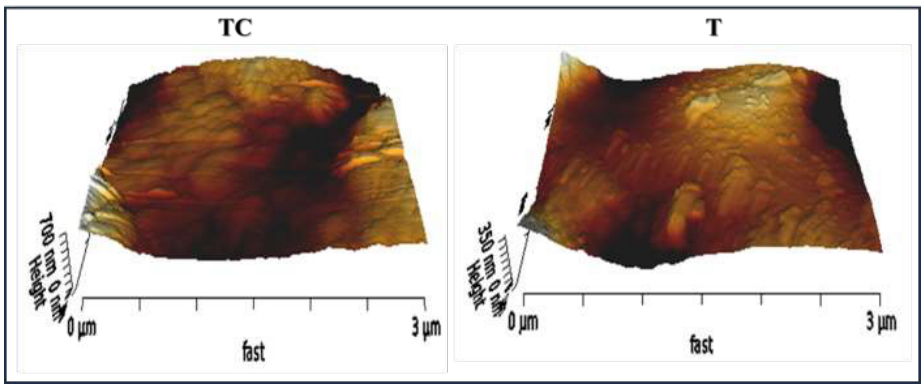

Fig. 3- AFM images (scan sizes of 3×3 µm) for T and TC samples.

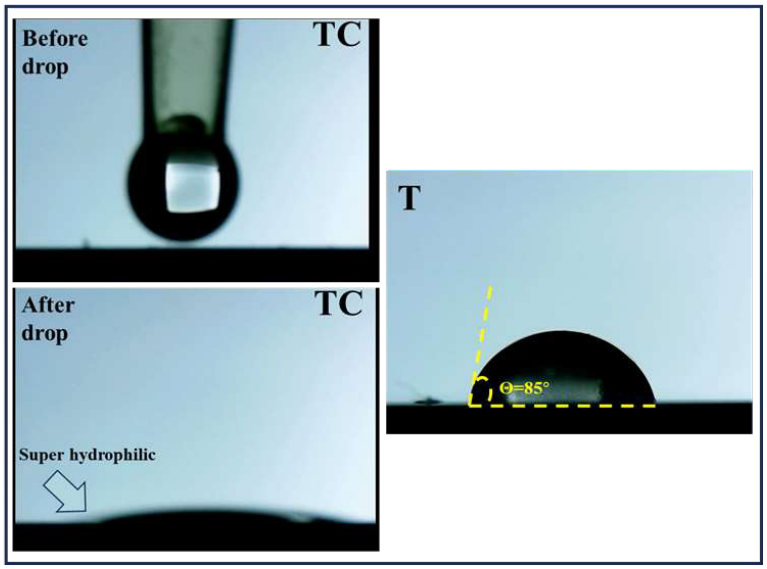

Fig. 4- Wettability test for TC and T samples.

both radical and non-radical pathways during PDS activation [26,27]:

$$S_2O_8^{2-} + H^+ \rightarrow HS_2O_8^- \quad \text{(1-non-radical)}$$

$$HS_2O_8^- \rightarrow SO_4^{2-} + H^+ + SO_4^{\bullet -} \quad \text{(2-non-radical)}$$

$$SO_4^{\bullet -} + H_2O \rightarrow HO^\bullet + HSO_4^- \quad \text{(3-radical)}$$

$$S_2O_8^{2-} \rightarrow 2SO_4^{\bullet -} + {}^1O_2 \quad \text{(4-non-radical)}$$

Additionally, the decomposition of persulfate generates hydrogen ions (H^+), which contribute to the acidic environment of the reaction system (Eqs. (5,6)) [8]:

$$2H_2O + 2S_2O_8^{2-} \rightarrow 4HSO_4^- + O_2^- \quad \text{(5-non-radical)}$$

$$HSO_4^- \rightarrow SO_4^{2-} + H^+ \quad \text{(6-non-radical)}$$

In the case of PMS in the photoreaction, the results closely resemble those of the previous oxidant. Given that the radical species generated by both oxidants are likely similar, methanol and tert-butanol were utilized as trapping agents to more precisely examine and identify the presence or participation of $HO^\bullet$ and $SO_4^{\bullet -}$. As reported in the literature [8], the reaction rate constants of methanol and tert-butanol with hydroxyl radicals $HO^\bullet$ are comparable, with ($k_{HO^\bullet/Methanol}$= 9.7 × 10^8 $M^{-1}.s^{-1}$ and $k_{HO^\bullet/Tert\text{-}butanol}$= 3.8–7.6 × 10^8 $M^{-1}.s^{-1}$). However, the kinetic constant describing the interaction of methanol with sulfate radicals $SO_4^{\bullet -}$ is noticeably higher (1.6–7.7 × 10^7 $M^{-1}.s^{-1}$) compared to that of tert-butanol with $SO_4^{\bullet -}$ (k = 4.0–9.1 × 10^5 $M^{-1}.s^{-1}$). This difference makes methanol a more effective trapping agent for $SO_4^{\bullet -}$ than tert-butanol. Therefore, to assess the effect of $SO_4^{\bullet -}$, same concentration of both scavengers was used. As perceived in Fig. 5(c), the addition of methanol to the solution caused the Cr^{6+} photoreduction efficiency to decrease to 32%. In contrast, when tert-butanol was added, the efficiency increased to 74%. These results confirm the production of both sulfate radicals $SO_4^{\bullet -}$ and hydroxyl radicals $HO^\bullet$, with $SO_4^{\bullet -}$ representing a dominant part in the Cr^{6+} photoreduction process. The difference in inhibition behavior between the two scavengers is attributed to methanol's greater ability to scavenge sulfate radicals compared to tert-butanol. Moreover, the kinetic behavior of both scavengers was plotted in Fig. 5(d), validating previous results.

Similar to PDS, PMS activation also proceeds through both radical and non-radical mechanisms. As an oxidant, PMS could act as an electron acceptor in photoreduction reactions. In the non-radical mechanism, electrons transferred from the coating to PMS appear to generate $SO_4^{\bullet -}$ and $HO^\bullet$, as described in Eqs. (7,8). Furthermore, the holes produced in the VB interact with PMS, leading to the formation of $SO_5^{\bullet -}$ radical, as outlined in Eq. 9 [28,29]:

$$HSO_5^- + e^- \rightarrow OH^- + SO_4^{\bullet -} \quad \text{(7-non-radical)}$$

$$HSO_5^- + e^- \rightarrow HO^\bullet + SO_4^{2-} \quad \text{(8-non-radical)}$$

$$HSO_5^- + h^+ \rightarrow H^+ + SO_5^{\bullet -} \quad \text{(9-non-radical)}$$

Meanwhile, the solution pH is an essential variable influencing the production process/rate and the distribution of $SO_4^{\bullet -}$ species and hydroxy complexes on the surface of the catalyst [30]. Additionally, OH^-/H_2O can be relatively oxidized into hydroxyl radicals $HO^\bullet$ by $SO_4^{\bullet -}$ and/or HSO_5^- within the (3–9) pH range, as described in Eqs. (10-14).

$$HSO_5^- + SO_5^{2-} \rightarrow H^+ + 2SO_4^{2-} + O_2 \quad \text{(10-non radical)}$$

$$SO_4^- + OH^- \rightarrow HO^\bullet + SO_4^{2-} \quad K = (6.5 \pm 1.0) \times 10^7\ M^{-1}S^{-1}$$

(11-nan-radical)

$$SO_4^- + H_2O \rightarrow HO^\bullet + SO_4^{2-} + H^+ \quad K[H_2O] < (1.0) \times 10^3\ M^{-1}S^{-1}$$

(12-non-radical)

$$SO_4^- + H_2O \rightarrow HO^\bullet + HSO_4^- \quad \text{(13-non-radical)}$$

$$HSO_4^- + OH^- \rightarrow 2HO^\bullet + SO_4^{2-} + H^+ \quad \text{(14-non-radical)}$$

PMS may shift from non-radical mechanisms to radical ones upon activation. It releases H^+ ions, which acidify the solution, thereby enhancing the oxidative capacity of Cr^{6+}. Based on these acidic circumstances, the redox potential of Cr^{6+} is approximately 1.10 V, while the redox potentials of superoxide radicals $O_2^{\bullet -}$ and singlet oxygen $^1O_2$ are about 0.89 V and 0.81 V, respectively [31].

The recombination of $HO^\bullet$ radical can lead to the formation of H_2O_2[32]. Subsequently, hydrogen peroxide H_2O_2 interacts with sulfate radicals $SO_4^{\bullet -}$ to produce hydroperoxyl radicals $HO_2^\bullet$ (Eq. 15) [33].

$$SO_4^{\bullet -} + H_2O_2 \rightarrow HO_2^\bullet + HSO_4^- \quad \text{(15-radical)}$$

Also, the radicals produced in Eqs. (7-9) lead to the formation of the $SO_5^{\bullet -}$ radical, as outlined in Eqs. (16,17). Owing to their rapid reaction rate, the recombination of $SO_5^{\bullet -}$ radicals happen swiftly, giving rise to singlet oxygen ($^1O_2$) through an alternative pathway, as described in Eq. 18 [33].

$$HSO_5^- + HO^\bullet \rightarrow H_2O + SO_5^{\bullet -} \quad \text{(16-radical)}$$

$$HSO_5^- + SO_4^{\bullet -} \rightarrow SO_5^{\bullet -} + HSO_4^- \quad \text{(17-radical)}$$

$$SO_5^{\bullet -} + SO_5^{\bullet -} \rightarrow S_2O_8^{2-} + {}^1O_2 \qquad (18\text{-radical})$$

The self-scavenging influence (Eq. 19) is not important as long as the concentration of $SO_4^{\bullet -}$ stays low, since $SO_4^{\bullet -}$ is rapidly consumed in oxidation reactions.

$$SO_4^{\bullet -} + SO_4^{\bullet -} \rightarrow S_2O_8^{2-} \qquad (19\text{-radical})$$

Based on the findings from the photocatalytic activation of PMS and PDS, a unified reaction pathway of Cr^{6+} photoreduction, with the TC coating serving as the activator under visible

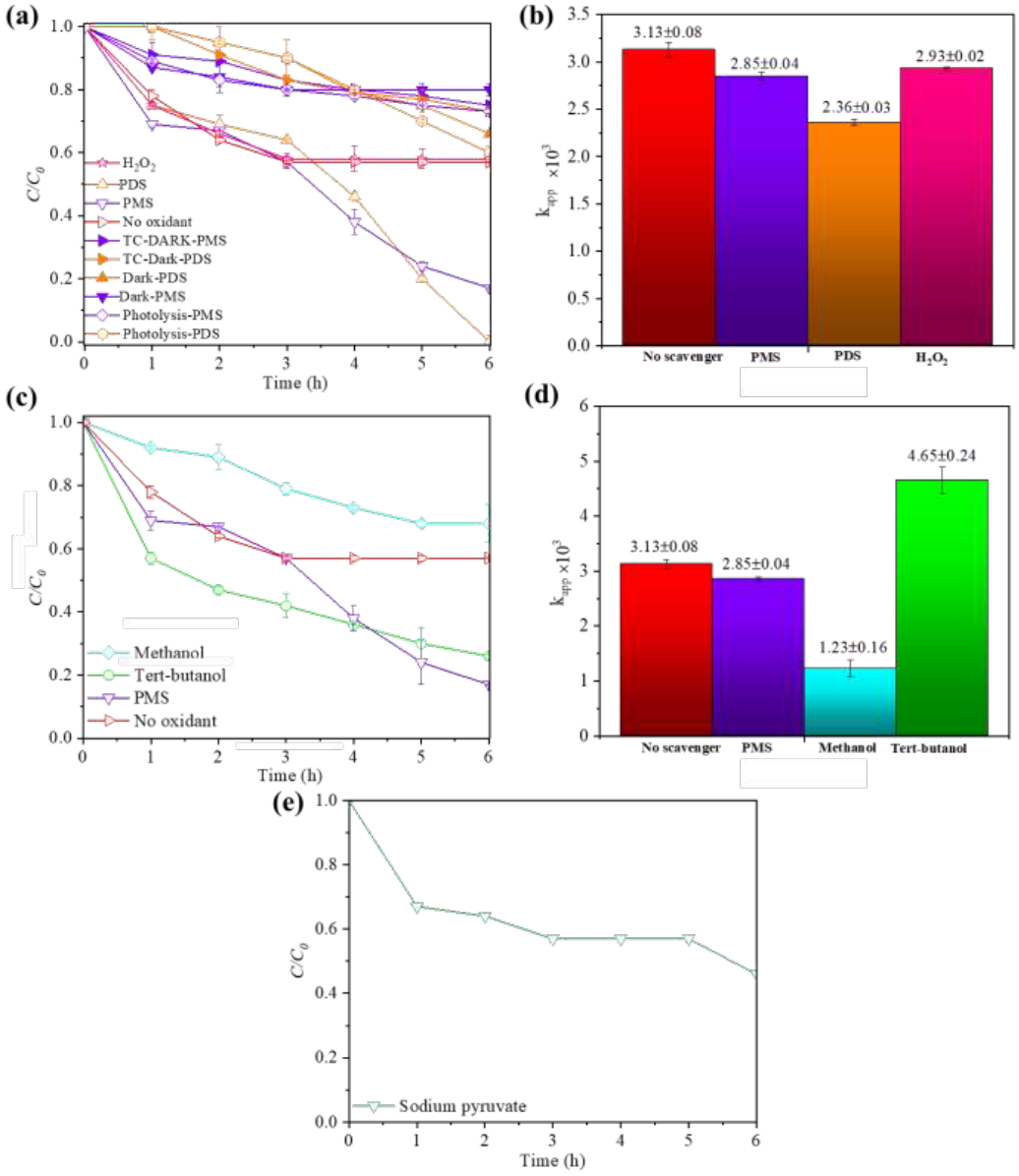

Fig. 5- Evaluation of the photocatalytic Cr^{6+} reduction performance using the TC coating under visible light, (a) Comparison of Cr^{6+} removal efficiency under dark and visible light conditions across different oxidants, (b) The corresponding apparent pseudo-first-order rate constants (k), (c) The impact of radical scavengers, methanol (MeOH) and tert-butanol (TBA), on Cr^{6+} removal in the TC-PMS system, (d) The calculated reaction rate constants for the scavenger experiments and (e) sodium pyruvate scavenger for H_2O_2. Experimental conditions: initial Cr^{6+} concentration, $[Cr]_0$ = 5 mg/L; initial oxidant concentration, [PMS, PDS, $H_2O_2]_0$ = 5 mM; scavengers' concentration for PMS and H_2O_2, 0.01M, 9.1mM respectively.

light illumination, is proposed. Fig. 6, provides a schematic representation, encompassing relevant reactive oxygen species whose roles in Cr^{6+} photoreduction have been either confirmed or hypothesized. The radical and non-radical pathways are distinguished using two different colors, corresponding to the specific reactions involved. The tip of each arrow denotes the resulting product of the respective reaction sequence. The only special feature in Fig. 6 is the intersection marked with a plus symbol, which indicates the simultaneous presence of both reactive species at that point in the mechanism.

Finally, the influence of PMS and PDS activation mediated by the TC coating on the photoactivity rate constant of Cr^{6+} was compared, as seen in Fig. 5(b). Both the TC/PMS and TC/PDS systems demonstrated nearly similar Cr^{6+} reduction activity under dark and visible light circumstances. The interactive influence of the components contributing to the reaction was analyzed using rate constants, as detailed in our prior study [34]. Table 1 provides the synergy indices corresponding to PMS and PDS activation, together with the rate constants obtained for the TC coating. The synergy values for the TC/PMS/Vis and TC/PDS/Vis systems were calculated to be 0.60 and 0.90, respectively. These results highlight the significant advantage of using the TC catalyst in PMS and PDS-enhanced Cr^{6+} photoreduction, achieving saturation in 6 h compared to the 3-hour saturation observed with the T sample alone.

H_2O_2 possesses a dual redox nature, enabling it to participate in both oxidation and reduction reactions. As an oxidant, it can accept electrons [$E^0(H_2O_2/H_2O)$= 1.77 V], while as a reductant it donates electrons [$E^0(O_2/ H_2O_2)$ = 0.68 V]. This dual functionality allows H_2O_2 to drive the interconversion between Cr^{3+} and Cr^{6+}species. Specifically, the interplay of the Cr^{6+}/Cr^{3+} and O_2/H_2O_2 redox pairs suggests that H_2O_2 promotes the oxidation of Cr^{3+} to Cr^{6+} at alkaline pH (> 8), whereas under acidic or near-neutral conditions it favors the reduction of Cr^{6+} to Cr^{3+} [35]. Although the solution pH was around 9, as could be seen in Fig. 5(a), H_2O_2 acted neither as an oxidant nor a reductant. The neutral—or, in other words, ineffective—behavior of this oxidant was also confirmed using the sodium pyruvate scavenging test (Fig. 6(e)). Considering the small pH difference between the experimental conditions and the oxidation zone discussed above, it can be inferred that the likelihood of oxidation influencing chromium increases with the basicity of the solution. Moreover, as the system deviates further from the defined oxidation and reduction zones, the behavioral distinction between these regions becomes more pronounced.

Table. 1- Synergistic factor associated with PMS and PDS activation by the TC sample under visible illumination

Conditions	$k \times 10^3$ (min^{-1})	Synergistic factor
Photolysis	**0.65 (±0.01)**	
Photolysis/PMS	**1.21 (±0.01)**	
PMS/Dark	**0.80 (±0.09)**	
PDS/Dark	**0.90 (±0.17)**	-
Photolysis/PDS	**0.60 (±0.15)**	
TC/Dark	**0.75 (±0.10)**	
TC/Vis	**3.13 (±0.33)**	
TC/PMS/Dark	**0.96 (±0.15)**	
TC/PMS/Vis	**2.85 (±0.04)**	**0.6**
TC/PDS/Dark	**1.08 (±0.26)**	
TC/PDS/Vis	**2.36 (±0.03)**	**0.9**

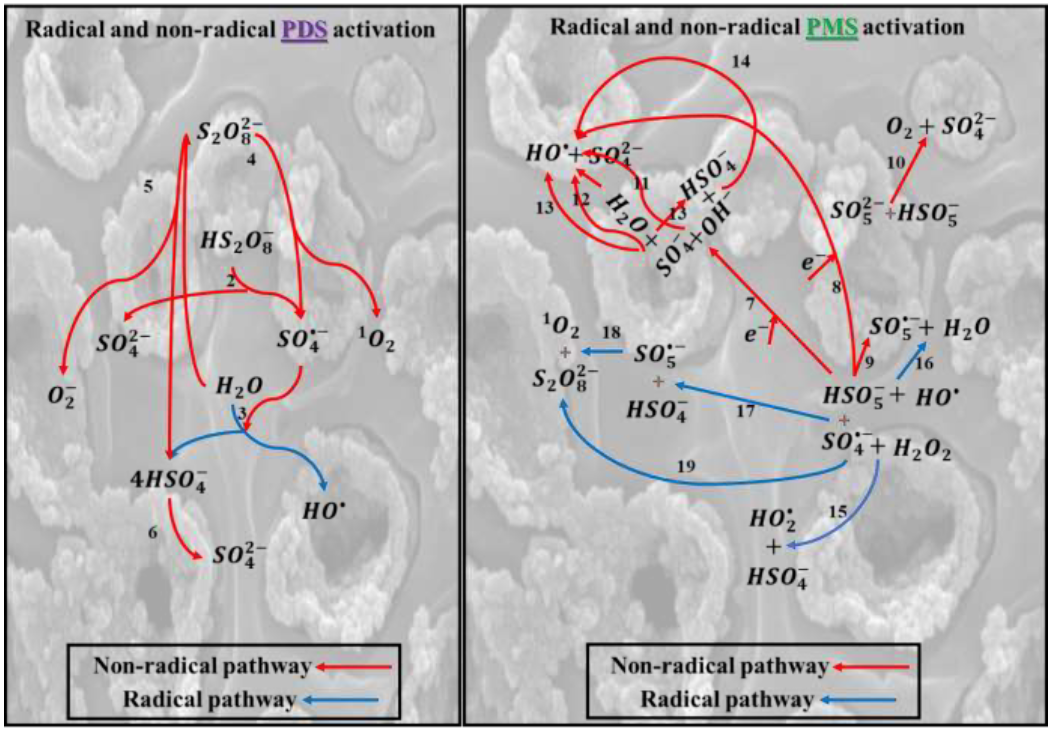

Fig. 6- The anticipated photocatalytic pathway of the TC coating under visible light exposure, incorporating PMS and PDS.

4. Conclusion and future prospective

In summary, a hydrothermally synthesized $TiO_2/CuWO_4$ coating demonstrated high efficacy for visible-light Cr^{6+} photoreduction via synergistic radical and non-radical mechanisms. Material analyses revealed that $CuWO_4$ incorporation drastically increased surface roughness (100% increment) and imparted super hydrophilic character (from 85° to near zero degrees). The photocatalytic activity was governed by ($SO_4^{\bullet-}$, and $HO^{\bullet}$ radicals), with PDS proving to be a more effective than PMS by 0.9 calculated synergistic factor compared to that of 0.6. It has to be mentioned that, ozone, periodate (and its associated iodate and periodate radicals), and percarbonate may also be considered in future research to determine the most appropriate oxidant for Cr photoreduction.

Acknowledgments

This work has been supported by the Center for International Scientific Studies & Collaboration (CISSC), Ministry of Science Research and Technology of Iran under Project No. 4030560.

References

1. R. Chaharmahali, A. Fattah-alhosseini, M. Karbasi, D. Dastan, S. Giannakis, Synergistic effects of PEO and hydrothermal post-treatment on the photocatalytic behavior of TiO_2/Bi_2WO_6 coatings: Distinguishing between Type II and Z-Scheme heterojunctions, J. Environ. Chem. Eng. 13 (2025) 116583.
2. R. Chaharmahali, A. Fattah-alhosseini, M. Karbasi, Unveiling enhanced photocatalytic behavior: Plasma electrolytic oxidation for TiO_2/Bi_2WO_6 heterojunction coatings to enhance the photocatalytic degradation of methylene blue under visible light, Ceram. Int. 51 (2025) 11255–11266.
3. S.J. McGrane, Impacts of urbanisation on hydrological and water quality dynamics, and urban water management: a review, Hydrol. Sci. J. 61 (2016) 2295–2311.
4. A. Fattah-alhosseini, M. Karbasi, H. Bahramian, A thorough investigation of the utilization of metal-organic framework (MOF) coated titanium dioxide in photocatalytic applications: A review, Appl. Surf. Sci. Adv. 18 (2023) 100504.
5. L.B. Khalil, W.E. Mourad, M.W. Rophael, Photocatalytic reduction of environmental pollutant Cr(VI) over some semiconductors under UV/visible light illumination, Appl. Catal. B Environ. 17 (1998) 267–273.
6. D. Zhu, Q. Zhou, Action and mechanism of semiconductor photocatalysis on degradation of organic pollutants in water treatment: A review, Environ. Nanotechnology, Monit. Manag. 12 (2019) 100255.
7. Y. Cai, H. Shu, F. Yu, Y. Yang, Molecular sieving of semiconductive NTU-9 coatings on titanium dioxide nanowire arrays: Augmented yet selective photoelectrochemical response enabled by boosting charge separation and transfer in confined

space, J. Colloid Interface Sci. 630 (2023) 523–533.
8. P. He, J. Zhu, Y. Chen, F. Chen, J. Zhu, M. Liu, K. Zhang, M. Gan, Pyrite-activated persulfate for simultaneous 2,4-DCP oxidation and Cr(VI) reduction, Chem. Eng. J. 406 (2021) 126758.
9. S. Stojadinović, N. Tadić, N. Radić, B. Grbić, R. Vasilić, CdS particles modified TiO_2 coatings formed by plasma electrolytic oxidation with enhanced photocatalytic activity, Surf. Coatings Technol. 344 (2018) 528–533.
10. J. Wu, X. Jiang, Y. Zhang, Q. Fu, C. Pan, Preparation of high-concentration substitutional carbon-doped TiO2 film via a two-step method for high-performance photocatalysis, RSC Adv. 8 (2018) 36691–36696.
11. Y.Q. Wang, X.D. Jiang, C.X. Pan, In Situ Preparation of TiO_2 Composite Layer upon Ti Alloy Substrate Using Micro-Arc Oxidation and its Photocatalytic Property, Mater. Sci. Forum 663–665 (2010) 3–11.
12. M.S. Sharifiyan, A. Fattah-alhosseini, M. Karbasi, Photocatalytic evaluation of hierarchical TiO_2/WO_3 hybrid coating created by PEO/hydrothermal method, Appl. Surf. Sci. Adv. 18 (2023) 100541.
13. H. Bahramian, A. Fattah-alhosseini, M. Karbasi, E. Nikoomanzari, S. Giannakis, Synergy of Cu^{2+}-$Cu(OH)_2$-CuO with TiO_2 coatings, fabricated via plasma electrolytic Oxidation: Insights into the multifaceted mechanism governing visible light-driven photodegradation of tetracycline, Chem. Eng. J. 476 (2023) 146588.
14. P. Raizada, S. Sharma, A. Kumar, P. Singh, A.A. Parwaz Khan, A.M. Asiri, Performance improvement strategies of $CuWO_4$ photocatalyst for hydrogen generation and pollutant degradation, J. Environ. Chem. Eng. 8 (2020) 104230.
15. H. Salimi, A. Fattah-alhosseini, M. Karbasi, E. Nikoomanzari, Development of WO_3-incorporated porous ceramic coating: A key role of WO_3 nanoparticle concentration on methylene blue photodegradation upon visible light illumination, Ceram. Int. 49 (2023) 32181–32192.
16. E. Nikoomanzari, M. Karbasi, W. C.M.A. Melo, H. Moris, K. Babaei, S. Giannakis, A. Fattah-alhosseini, Impressive strides in antibacterial performance amelioration of Ti-based implants via plasma electrolytic oxidation (PEO): A review of the recent advancements, Chem. Eng. J. 441 (2022) 136003.
17. R. Hosseini, A. Fattah-alhosseini, M. Karbasi, Photodegradation of tetracycline using surface oxygen vacancy-enriched PEO coating under visible light, Surfaces and Interfaces 42 (2023) 103311.
18. M. Kaseem, S. Fatimah, N. Nashrah, Y.G. Ko, Recent progress in surface modification of metals coated by plasma electrolytic oxidation: Principle, structure, and performance, Prog. Mater. Sci. 117 (2021) 100735.
19. M.S. Sharifiyan, A. Fattah-alhosseini, M. Karbasi, Optimizing the hydrothermal post-treatment process for a TiO_2/WO_3 hybrid coating to enhance the photocatalytic degradation of methylene blue under visible light, Ceram. Int. 49 (2023) 35175–35185.
20. H. Bahramian, A. Fattah-alhosseini, M. Karbasi, M. Kaseem, M. Sillanpää, B. Dikici, Influence of $CuWO_4$-induced heterostructures on porous TiO_2 ceramic coatings for Cr^{6+} reduction, Process Saf. Environ. Prot. 202 (2025) 107814.
21. A. Saberyoun, A. Fattah-alhosseini, M. Karbasi, R. Hosseini, M. Kaseem, Boosting the visible-light-driven photocatalytic efficiency in porous Cu/TiO_2 ceramic coatings, Ceram. Int. 50 (2024) 31313–31325.
22. T.T. My Hang, N.H. Thao Vy, N.T. Hanh, T.-D. Pham, L.T. Hoang Yen, Facile synthesis of copper tungstate ($CuWO_4$) for novel photocatalytic degradation of tetracycline under visible light, Sustain. Chem. Pharm. 21 (2021) 100407.
23. A. Santos-Coquillat, M. Mohedano, E. Martinez-Campos, R. Arrabal, A. Pardo, E. Matykina, Bioactive multi-elemental PEO-coatings on titanium for dental implant applications, Mater. Sci. Eng. C 97 (2019) 738–752.
24. A. Fattah-Alhosseini, M.K. Keshavarz, M. Molaei, S.O. Gashti, Plasma Electrolytic Oxidation (PEO) Process on Commercially Pure Ti Surface: Effects of Electrolyte on the Microstructure and Corrosion Behavior of Coatings, Metall. Mater. Trans. A 49 (2018) 4966–4979.
25. W. Thongsuwan, T. Kumpika, P. Singjai, Effect of high roughness on a long aging time of superhydrophilic TiO_2 nanoparticle thin films, Curr. Appl. Phys. 11 (2011) 1237–1242.
26. J. Wang, S. Wang, Activation of persulfate (PS) and peroxymonosulfate (PMS) and application for the degradation of emerging contaminants, Chem. Eng. J. 334 (2018) 1502–1517.
27. X. Duan, H. Sun, Z. Shao, S. Wang, Nonradical reactions in environmental remediation processes: Uncertainty and challenges, Appl. Catal. B Environ. 224 (2018) 973–982.
28. P. Hu, M. Long, Cobalt-catalyzed sulfate radical-based advanced oxidation: A review on heterogeneous catalysts and applications, Appl. Catal. B Environ. 181 (2016) 103–117.
29. X. Zhou, Q. Zhao, J. Wang, Z. Chen, Z. Chen, Nonradical oxidation processes in PMS-based heterogeneous catalytic system: Generation, identification, oxidation characteristics, challenges response and application prospects, Chem. Eng. J. 410 (2021) 128312.
30. Y. Peng, H. Tang, B. Yao, X. Gao, X. Yang, Y. Zhou, Activation of peroxymonosulfate (PMS) by spinel ferrite and their composites in degradation of organic pollutants: A Review, Chem. Eng. J. 414 (2021) 128800.
31. W.-M. Yang, F. Liu, Y.-T. Jin, Z.-M. Dong, G.-C. Zhao, Efficient Reduction of Cr(VI) with Carbon Quantum Dots, ACS Omega 7 (2022) 23555–23565.
32. S. Mohammadi, G. Moussavi, S. Shekoohiyan, M.L. Marín, F. Boscá, S. Giannakis, A continuous-flow catalytic process with natural hematite-alginate beads for effective water decontamination and disinfection: Peroxymonosulfate activation leading to dominant sulfate radical and minor non-radical pathways, Chem. Eng. J. 411 (2021).
33. C. Zhu, Y. Zhang, Z. Fan, F. Liu, A. Li, Carbonate-enhanced catalytic activity and stability of Co_3O_4 nanowires for $1O_2$-driven bisphenol A degradation via peroxymonosulfate activation: Critical roles of electron and proton acceptors, J. Hazard. Mater. 393 (2020) 122395.
34. R. Hosseini, A. Fattah-alhosseini, M. Karbasi, S. Giannakis, Tailoring surface defects in Plasma Electrolytic Oxidation (PEO) treated 2-D black TiO_2: Post-treatment role, and intensification by peroxymonosulfate activation in visible light-driven photocatalysis, Appl. Catal. B Environ. 340 (2024) 123197.
35. A.D. Bokare, W. Choi, Advanced Oxidation Process Based on the Cr(III)/Cr(VI) Redox Cycle, Environ. Sci. Technol. 45 (2011) 9332–9338.